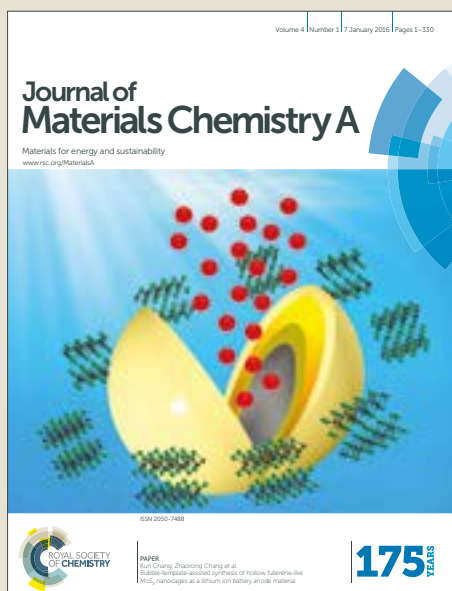


Journal of Materials Chemistry A

Accepted Manuscript



This article can be cited before page numbers have been issued, to do this please use: W. Gao, T. Liu, Z. Luo, L. Zhang, R. Ming, C. Zhong, W. Ma, H. Yan and C. Yang, *J. Mater. Chem. A*, 2019, DOI: 10.1039/C9TA00597H.



This is an Accepted Manuscript, which has been through the Royal Society of Chemistry peer review process and has been accepted for publication.

Accepted Manuscripts are published online shortly after acceptance, before technical editing, formatting and proof reading. Using this free service, authors can make their results available to the community, in citable form, before we publish the edited article. We will replace this Accepted Manuscript with the edited and formatted Advance Article as soon as it is available.

You can find more information about Accepted Manuscripts in the [author guidelines](#).

Please note that technical editing may introduce minor changes to the text and/or graphics, which may alter content. The journal's standard [Terms & Conditions](#) and the ethical guidelines, outlined in our [author and reviewer resource centre](#), still apply. In no event shall the Royal Society of Chemistry be held responsible for any errors or omissions in this Accepted Manuscript or any consequences arising from the use of any information it contains.

Regulating Exciton Bonding Energy and Bulk-Heterojunction Morphology in Organic Solar Cells via Methyl Functionalized Non-Fullerene Acceptors

Wei Gao,^{ab} Tao Liu,^c Zhenghui Luo,^a Lin Zhang,^d Ruijie Ming,^a Cheng Zhong,^{*a} Wei Ma,^d He Yan^{*c} and Chuluo Yang^{*ab}

Received 00th January 20xx,
Accepted 00th January 20xx

DOI: 10.1039/x0xx00000x

www.rsc.org/

Electron-deficient end groups (EGs) are very important for non-fullerene small molecule acceptors (NF-SMAs) to tune its absorption, energy levels and crystallization properties. Herein, we designed and synthesized three SMAs, namely BTTIC-0M, BTTIC-2M and BTTIC-4M, by adding methyl unit onto 2-(6-oxo-5,6-dihydro-4H-cyclopenta[c]thiophen-4-ylidene)malononitrile (CPTCN). Methyl with slight electron-donating ability significantly elevates the LUMO energy levels but does not seriously affect the bandgaps of CPTCN-based SMAs, which helps to reduce the energy loss (E_{loss}). In-depth dynamics theory simulations of donor-acceptor (D-A) complex reveal that exciton bonding energy (BE) can be fine-tuned through continuously increasing methyl onto the end group of SMAs. Methyl substituted EG reduces the driving force and also enhances the BE of charge transport (CT) state exciton, leading to a decrease in exciton dissociation efficiencies. However, we found that one methyl functionalized CPTCN enables PBDB-T:BTTIC-2M-based organic solar cells (OSCs) achieve highest power conversion efficiency (PCE) as high as 13.15%. Though PBDB-T:BTTIC-2M-based OSCs exhibit a slightly lower exciton dissociation efficiency than that of PBDB-T:BTTIC-0M, a more favorable superficial and internal morphology is attained in PBDB-T:BTTIC-2M bulk-heterojunction layer, which balances the electron and hole mobilities and diminishes the bimolecular recombination. Comparatively, BTTIC-4M failed to realize high performance owing to its adverse interactions with polymer chain and multiscale phase separation in the blend films. Actually, adjusting the amount of methyl on end group is to compromise the current-voltage losses within OSC devices with complicated contributions from absorption spectra, LUMO energy levels, exciton bonding energies and morphologies.

1. Introduction

Bulk-heterojunction (BHJ) organic solar cells (OSCs) composed of donor and acceptor¹⁻⁴ can be fabricated into flexible and large-area devices using high-throughput solution processing method, making them a promising photovoltaic technology.⁵ The past two decades have witnessed a rapid growth in the power conversion efficiencies (PCEs) of OSCs: from an initial PCE of less than 1% to a PCE of more than 12% in fullerene-based system today.⁶⁻²⁰ The tremendous advances in the field of OSCs can be attributed to the innovation of photoactive materials, device optimization and interface engineering. Emerging as a

new dawn, acceptor-donor-acceptor (A-D-A) type non-fullerene small molecule acceptors (NF-SMAs), featuring an electron-rich core end-capped with two electron-deficient groups, have caught a wide range of interests to make further PCE breakthroughs.²¹⁻⁶² The most representative example is 3,9-bis(2-methylene-(3-(1,1-dicyanomethylene)-indanone))-5,5,11,11-tetrakis(4-hexylphenyl)-dithieno[2,3-d':2',3'-d'']-s-indaceno[1,2-b:5,6-b']-dithiophene (ITIC) which was first reported by Zhan group.²³ Merits of such kind of molecules lie in their modifiable structures which have allowed precise optimization of the absorption spectra,²⁴⁻³⁶ the lowest unoccupied molecular orbital (LUMO)/highest occupied molecular orbital (HOMO) levels³⁷⁻³⁹ and the crystallization/aggregation properties.⁴⁰⁻⁵³ In the past three years, research progresses are so rapid that open-circuit voltage (V_{OC}) of over 1 V,⁵⁴ short-circuit current (J_{SC}) of 25 mA cm⁻²,^{29,55} fill factor (FF) of 78%^{44,51,56,57} and PCE of 14%^{36,51,56,58} have been achieved separately in single-junction devices via judicious molecular design.

It is well known that the PCE of an OSC device is equal to the product of V_{OC} , J_{SC} and FF, which means that the most straightforward way to improve the PCE is to increase these three parameters simultaneously. However, it is very challenging in current stage because of the trade-off between

^a Department of Chemistry and Hubei Key Lab on Organic and Polymeric Optoelectronic Materials, Wuhan University, Wuhan, 430072, People's Republic of China. E-mail: zhongcheng@whu.edu.cn, clyang@whu.edu.cn

^b Shenzhen Key Laboratory of Polymer Science and Technology, College of Materials Science and Engineering, Shenzhen University, Shenzhen 518060, China

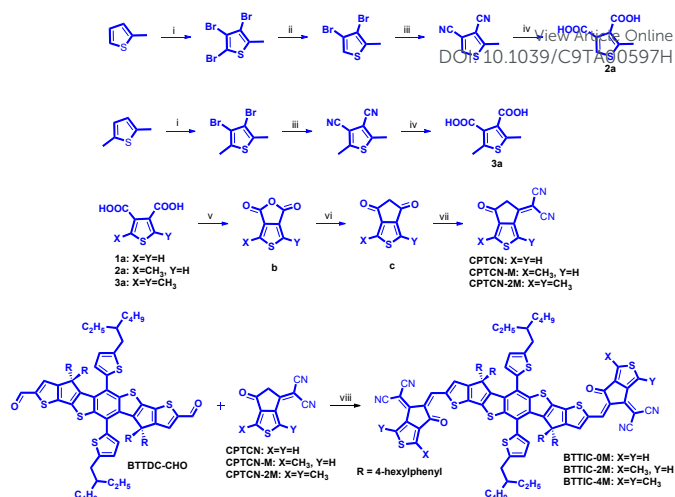
^c Department of Chemistry and Hong Kong Branch of Chinese National Engineering Research Center for Tissue Restoration & Reconstruction, Hong Kong University of Science and Technology, Clear Water Bay, Kowloon, Hong Kong. E-mail: hyan@ust.hk

^d State Key Laboratory for Mechanical Behavior of Materials, Xi'an Jiaotong University, Xi'an 710049, China

[†]Electronic Supplementary Information (ESI) available: materials synthesis; devices fabrications; SCLC measurements; AFM and ¹H and ¹³C NMR spectra. See DOI: 10.1039/x0xx00000x

V_{oc} and J_{sc} . Besides, although we compromise the loss of V_{oc} and J_{sc} in one cell, it is still difficult to control the active-layer morphology to obtain a better FF. Methyl, as a weak electron-donating group with a small steric effect, has been successfully introduced into the design of organic semiconductor materials.^{38,39} Theoretical calculations indicate that the LUMO level of the ITIC family is mainly determined by the end group. Therefore, replacing the hydrogen atom on the terminal group with a methyl weakens the electron-withdrawing ability of end group and thereby increases the LUMO energy level of the whole acceptor molecule, leading to a smaller energy loss (E_{loss}) without strongly affecting absorption.³⁹ Furthermore, the LUMO energy level of SMA can be finely adjusted by the number of methyl. It is worth mentioning that methyl reduces the reorganization energy between the packing fractions and thus effectively enhances crystallinity,^{38,39} which helps achieve a regular morphology and a high FF in OSCs.

Taken the advantages of methyl group into consideration, we applied this methyl substitution strategy on 2-(6-oxo-5,6-dihydro-4*H*-cyclopenta[*c*]thiophen-4-ylidene)malononitrile (CPTCN) which first reported by our group has been proved as a powerful end group to construct efficient SMAs.^{33,39-41,43,47-49} For instance, ITCPTC, as a CPTCN-based SMA, realized a PCE of 12.3% when paired with PM6.⁴³ Herein, we designed and synthesized three SMAs, BTTIC-0M, BTTIC-2M and BTTIC-4M, by stepwise methylation on the CPTCN. As the methyl group increases, the LUMO energy levels of BTTIC-0M, BTTIC-2M and BTTIC-4M were gradually increased without excessively reducing bandgap. When blended with a commercially available polymer PBDB-T, BTTIC-2M-based OSCs gained a better performance than their BTTIC-0M and BTTIC-4M counterparts: a high PCE up to 13.15% produced from a V_{oc} of 0.90 V, a J_{sc} of 19.40 mA cm⁻² and a FF of 75.3%. BTTIC-4M based OSCs exhibited a high V_{oc} but very low J_{sc} and FF. BTTIC-0M based OSCs exhibited a moderate PCE of 11.87%. To further explore the effect of methyl on device efficiency, we performed the dynamic theory simulations of donor-acceptor (D-A) complex. We found that methyl groups increase the charge transfer (CT) state energies and bandgaps (electronic affinity (EA)-ionization potential (IP)) of donor-acceptor (D-A) complex, causing an enhancement of bonding energies of CT state excitons especially for PBDB-T:BTTIC-4M and thus seriously affecting the exciton dissociation upon the D-A interface. Adding methyl group can optimize the superficial and internal morphology of the blends to balance the carrier mobility and reduce bimolecular recombination. Excessive methyl group causes multiple crystal phases and weakens intermolecular π - π stacking, which significantly affects the carriers transport and bimolecular recombination, and thus results in lower J_{sc} and FF in OSCs. Finally, this work provides a high-performance EG and gains insights into the important roles of exciton BE and bulk-heterojunction morphology on the performance of OSCs.



Scheme 1. The synthetic routes of end groups and SMAs. (i) Br₂, CHCl₃, refluxed; (ii) Zn, CH₃COOH, refluxed; (iii) CuCN, DMF, 180°C; (iv) KOH, (CH₂OH)₂, 200°C; (v) Ac₂O, refluxed; (vi) Ac₂O, Et₃N, tert-butyl 3-oxobutanoate, 80°C; (vii) malononitrile, KOAc, EtOH; (viii) Py, CHCl₃, 70°C.

2. Results and discussion

2.1. Synthesis

The detailed synthetic procedures of the end groups and SMAs are shown in **Scheme 1**. The 3,4-dibromo compound of 2,5-dimethylthiophene (or 2-methylthiophene) first underwent a nucleophilic substitution reaction and then hydrolyzed to give compound **3a** (or **2a**). One of the more general methods for synthesizing such active methylene compounds (CPTCN, CPTCN-M and CPTCN-2M) is to convert the dicarboxylic compound (compound **a**) into an acid anhydride (compound **b**), and then the anhydride reacted with *tert*-butyl 3-oxobutanoate to obtain 4*H*-cyclopenta[*c*]thiophene-4,6(5*H*)-dione derivatives (compound **c**). CPTCN-2M (CPTCN or CPTCN-M) was yielded through a condensation reaction between 1,3-dimethyl-4*H*-cyclopenta[*c*]thiophene-4,6(5*H*)-dione and malononitrile. Facile Knoevenagel condensation reactions between BTTDC-CHO and CPTCN, CPTCN-M and CPTCN-2M were conducted to receive BTTIC-0M, BTTIC-2M and BTTIC-4M in a high yield, respectively. The three SMAs were fully characterized by ¹H/¹³C NMR and Mass spectrometry (MS), and all shows excellent solubility in commonly-used solvents, meeting the basic requirements for OSCs devices.

2.2. Optical and electrochemical properties

The UV-vis absorption of BTTIC-0M, BTTIC-2M and BTTIC-4M in chloroform solution, neat films and blend films were shown in **Fig. S1**, **1a** and **1b**, respectively. In the dilute chloroform solution (10⁻⁶ M⁻¹), BTTIC-0M, BTTIC-2M and BTTIC-4M exhibit wide absorption ranges with maximal absorption located at 727, 723 and 714 nm, and large molar extinction coefficients of 2.95 × 10⁵, 2.33 × 10⁵ and 2.20 × 10⁵ M⁻¹ cm⁻¹, respectively. As the amount of methyl group increases, the absorption spectra of these SMAs gradually blue shift, and the molar extinction coefficient decreases (**Table 1**). A large red-shift of

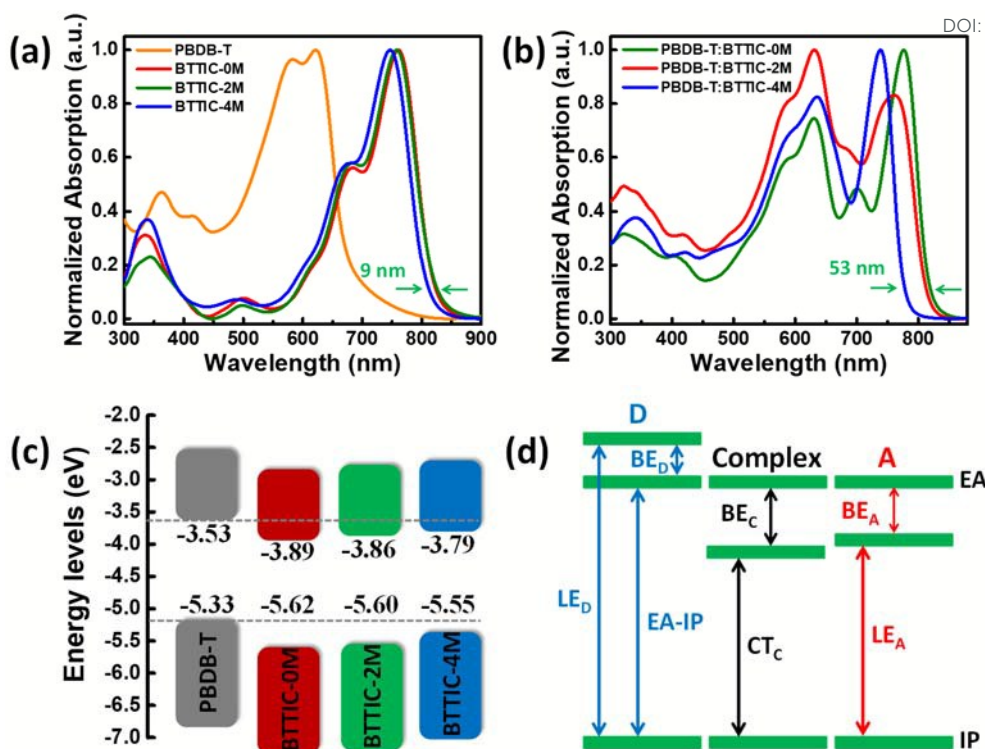


Fig. 1 a) The normalized UV-vis absorption spectra of PBDB-T, BTTIC-0M, BTTIC-2M and BTTIC-4M neat films. b) The normalized UV-vis absorption spectra of PBDB-T:BTTIC-0M, PBDB-T:BTTIC-2M and PBDB-T:BTTIC-4M blend films. c) Energy levels of PBDB-T, BTTIC-0M, BTTIC-2M and BTTIC-4M. d) Schematic diagram of the relationship between local state (LE) energy, charge transfer state (CT) energy, exciton binding energy (BE), electronic affinity (EA) and ionization potential (IP) of D-A complex.

Table 1 The basic properties of BTTIC-0M, BTTIC-2M and BTTIC-4M.

Acceptor	λ_{\max}^a (nm)	λ_{onset}^a (nm)	ϵ_{\max}^b ($\text{M}^{-1} \text{cm}^{-1}$)	λ_{\max}^b (nm)	λ_{onset}^b (nm)	E_g^{optc} (eV)	HOMO ^d (eV)	LUMO ^d (eV)	μ_e^e ($\text{cm}^2 \text{V}^{-1} \text{s}^{-1}$)
BTTIC-0M	727	787	2.95×10^5	761	842	1.47	-5.62	-3.89	6.73×10^{-4}
BTTIC-2M	723	784	2.33×10^5	758	841	1.47	-5.60	-3.86	8.19×10^{-4}
BTTIC-4M	714	779	2.20×10^5	747	833	1.49	-5.55	-3.79	9.38×10^{-4}

^aIn chloroform solution. ^bIn neat film. ^cCalculated from empirical formula: $E_g^{\text{opt}} = 1240/\lambda_{\text{onset}}$. ^dUsing cyclic voltammetry (CV) method. ^eMeasured by space charge limited current (SCLC) method based on electron-only device with a structure of ITO/ZnO/acceptor/ZrAcac/Al.

absorption edge from solution to films and strong vibration shoulder peaks can be observed in film absorption, indicating intense intermolecular packing in these neat films. The absorption edges of BTTIC-0M, BTTIC-2M and BTTIC-4M neat films are estimated to be 842, 841 and 833 nm, corresponding to the optical bandgaps of 1.47, 1.47 and 1.49 eV, respectively. Interestingly, a special phenomenon occurred in the blend film that the absorption of PBDB-T:BTTIC-4M blend displays a very large blue shift of over 50 nm relative to that of PBDB-T:BTTIC-0M blend while the absorption of PBDB-T:BTTIC-2M is slightly blue-shifted compared with that of PBDB-T:BTTIC-0M (Fig. 1b). We suspected that BTTIC-4M has interactions with PBDB-T polymer chain due to the large spatial steric hindrance effect between dicyano group and the ipsilateral methyl group in CPTCN-2M, disrupting the ordered packing of PBDB-T:BTTIC-4M blend (this issue will be discussed below). Cyclic voltammetry (CV) measurements were conducted to test the electrochemical properties of three SMAs. By calculating the CV plots, the

LUMO/HOMO energy levels were measured to be -3.89/-5.62 eV for BTTIC-0M, -3.86/-5.60 eV for BTTIC-2M and -3.79/-5.55 eV for BTTIC-4M. Adding two methyl groups into BTTIC-0M elevates its LUMO energy level by 0.03 eV without substantially narrowing its absorption. Although the addition of four methyl groups into BTTIC-0M causes a blue shift of 9 nm (about 0.007 eV), the LUMO energy level is significantly promoted by 0.07 eV, which enhances the V_{OC} and thus reduces the E_{loss} ($E_{\text{loss}} = E_g^{\text{opt}} - eV_{\text{OC}}$).

2.3. Theoretical calculation

To gain deep insights into the role of methyl, in-depth theoretical calculations on both single and dimer molecules of these SMAs were performed (Fig. 2). The long alkyl chains were simplified to be methyl groups. The molecular geometries were optimized at B3LYP/def2-SVP level by using ORCA 4.0 program with RIJCOSX approximation. Grimme's D3 dispersion correction with Becke-Johnson damping and

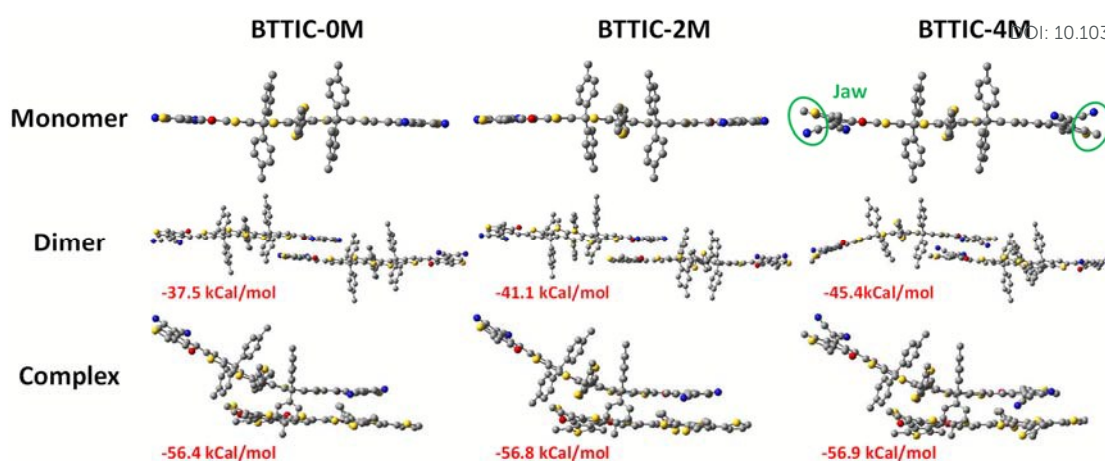


Fig. 2 Theoretical calculation results of single and dimer molecules of three SMAs and D-A complex.

Grimme's geometrical counterpoise correction (gCP) were used during the optimization. The wave functions were obtained at B3LYP/6-31G(d,p) level by using Gaussian09 program. The calculated LUMO/HOMO energy levels are -3.65/-5.74 eV for BTTIC-0M, -3.60/-5.71 eV for BTTIC-2M and -3.51/-5.63 eV for BTTIC-4M, which consist with the CV results and suggest that methyl effectively promotes LUMO energy levels of SMAs. The dihedral angles between end group and core of BTTIC-0M, BTTIC-2M and BTTIC-4M are 1.1°, 0.5° and 2.7°, respectively. BTTIC-2M exhibits better planarity than BTTIC-0M and BTTIC-4M, which is beneficial to π - π stacking and electron transport. The ipsilateral methyl and cyano groups in BTTIC-4M cause a large steric effect with dihedral angle up to 40.7°, much greater than that of BTTIC-2M (0.6°). This larger steric hindrance is like a jaw that may provide a possibility for interaction with polymer chain (Fig. 2a). The optimal geometry configurations of dimer molecules of three SMAs are displayed in Fig. 2b. The dimer molecules prefer an anti-parallel stacking form with the end groups as the main stacking units, which is conducive to the extension of the π - π stacking. The intermolecular interaction energies of BTTIC-0M, BTTIC-2M and BTTIC-4M dimers were calculated to be -37.5, -41.1 and -45.4 kcal mol⁻¹, respectively. Adding methyl groups can significantly reduce molecular reorganization energy and thus have a stronger tendency for intermolecular stacking. Although BTTIC-4M exhibits a lowest molecular binding energy, poor planarity of the whole molecular skeleton may affect the regularity of the intermolecular packing. Hence, BTTIC-2M possess a better crystallization/aggregation property than that of BTTIC-0M or BTTIC-4M in their neat and blend films.

The ultrafast exciton dissociation provides a solid foundation for organic photovoltaic (OPV) technology, which dominates over all other photophysical processes. It is generally acknowledged that the exciton dissociation is related to the exciton binding energy and driving force provided by the energy offsets between the LUMO (and/or HOMO) of donor and acceptor in the donor-acceptor (D-A) interface. To better understand the impact of methyl on this process, we simulated the D-A complexes via molecular dynamics to evaluate the

exciton bonding energy of these SMAs. The repeating unit of PBDB-T stacks upon a half wing of SMA with benzo[1,2-c:4,5-c']dithiophene-4,8-dione (BDD) moiety on the central core of SMA and benzo[1,2-b:4,5-b']dithiophene (BDT) moiety on the end group of SMA in the optimal conformation of these D-A complexes. These D-A complexes have nearly the same bonding energy of about -56 kcal mol⁻¹ (Fig. 2c), which offers an indirect evidence for the occurrence of interactions between BTTIC-4M and PBDB-T because the parallel stacking between three SMAs and PBDB-T exhibits the same bonding energy. The relationships between local state (LE) energy, charge transfer state (CT) energy, exciton binding energy (BE), electronic affinity (EA) and ionization potential (IP) of D-A complex were depicted in Fig. 1d. The CT energies of D-A complexes based on BTTIC-0M, BTTIC-2M and BTTIC-4M were calculated to be 1.38, 1.40 and 1.46 eV, respectively. The EAs/IPs of D-A complexes were -3.54/-5.46 eV for PBDB-T:BTTIC-0M, -3.51/-5.45 eV for PBDB-T:BTTIC-2M and -3.44/-5.45 eV for PBDB-T:BTTIC-4M, corresponding to the bandgaps (EA-IP) of 1.92, 1.94 and 2.01 eV, respectively. Therefore, the exciton bonding energy of CT states are 0.54, 0.54 and 0.55 eV for BTTIC-0M, BTTIC-2M and BTTIC-4M based D-A complexes. Methylation adjusts the energy of CT state, bandgap and BE energy of the D-A complex at the interface. Excessive methylation (BTTIC-4M) significantly weakens the CT state and widens the bandgap, resulting in a larger exciton bonding energy. From CV measurements, the values of $\Delta E_{\text{LUMO}} (E_{\text{LUMO}}^{\text{D}} - E_{\text{LUMO}}^{\text{A}}) / \Delta E_{\text{HOMO}} (E_{\text{HOMO}}^{\text{D}} - E_{\text{HOMO}}^{\text{A}})$ are 0.36/0.29 eV for BTTIC-0M, 0.33/0.27 eV for BTTIC-2M and 0.26/0.22 eV for BTTIC-4M. The PBDB-T:BTTIC-4M system exhibits larger exciton binding energy of CT state and the smaller energy offset than those of PBDB-T:BTTIC-0M and PBDB-T:BTTIC-2M, resulting in its lower exciton dissociation efficiency than the latter two systems. In addition, we also calculated the local state energies of PBDB-T and three SMAs in their D-A complex. The local state energies of BTTIC-0M, BTTIC-2M and BTTIC-4M are 1.59, 1.58 and 1.59 eV, corresponding to the exciton bonding energies of SMAs of 0.33, 0.36 and 0.42 eV, respectively, while the exciton bonding energies of PBDB-T in different D-A complex are negative

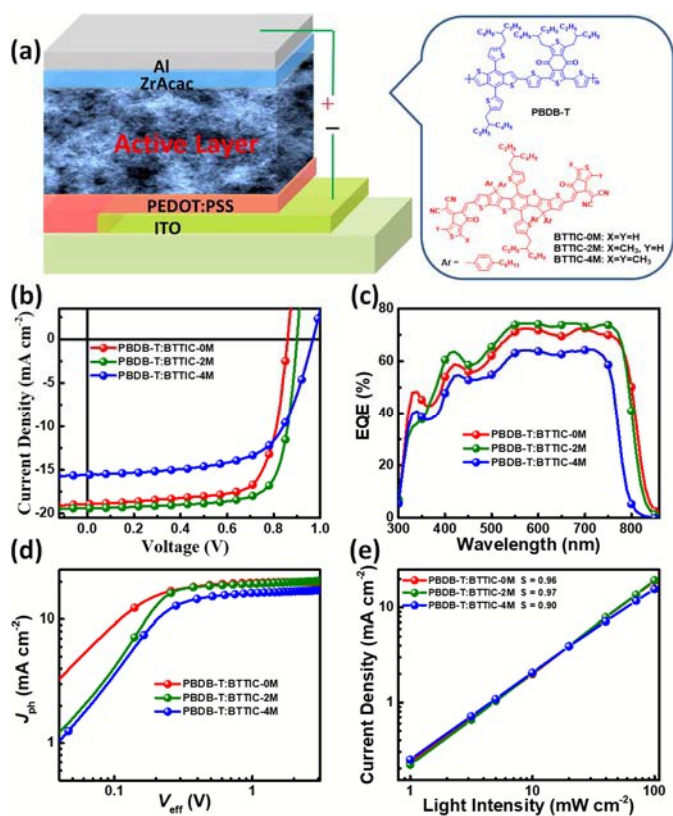


Fig. 3 a) Device configuration and the structures of investigated materials. b) *J*-*V* curves of three SMAs-based OSCs. c) Corresponding EQE spectra. d) *J*_{ph} versus *V*_{eff} curves. e) Light intensity dependence of *J*_{sc}.

values, indicating that the recombination of excitons occurs mainly in the acceptor and not in the donor. In fact, regulating the amount of methyl groups on SMAs is to balance the current-voltage loss in OSCs.

2.4. Photovoltaic performance

To understand the methyl effects on the photovoltaic performance, we fabricated a series of OSCs devices with a conventional configuration of indium tin oxide (ITO)/poly(3,4-ethylenedioxythiophene):poly(styrenesulfonate)(PEDOT:PSS)/PBDB-T:acceptor/zirconium acetylacetonate (ZrAcac)/Al (Fig. 3a). A wide-bandgap polymer PBDB-T was selected as donor due to its matched LUMO/HOMO energy levels and absorption spectrum with three studied SMAs. A commercially available ZrAcac served as cathode interfacial layer (CIL) for efficient charge extraction. Chloroform (CF) was chosen as the processing solvent considering its proper volatility, which is helpful for the formation of good morphology of OSCs. The optimal weight ratio of donor and acceptor (D:A) was 1:1 with the total concentration of blend solution being 16 mg ml⁻¹. Moreover, 1,8-diiodooctane (DIO) addition and annealing treatment were essentially required. The detailed device fabrication processes were described in supporting information. The best-performing current density-voltage (*J*-*V*) curves of three SMAs-based OSCs and corresponding external quantum efficiency (EQE) spectra are shown in Fig. 3b and 3c, and the key photovoltaic parameters are summarized in Table

2. OSCs based on PBDB-T:BTTIC-2M achieved a highest PCE of up to 13.15% with a *V*_{oc} of 0.90 V, a *J*_{sc} of 19.39 mA cm⁻² and a FF of 75.3%, which is significantly higher than those of PBDB-T:BTTIC-0M- (PCE of 11.87% with a *V*_{oc} of 0.86 V, a *J*_{sc} of 19.95 mA cm⁻² and a FF of 72.9%) and PBDB-T:BTTIC-4M- (PCE of 9.60% with a *V*_{oc} of 0.97 V, a *J*_{sc} of 15.67 mA cm⁻² and a FF of 63.7%) based OSCs. Adding two methyl groups into the BTTIC-0M not only increases the *V*_{oc} by 0.04V but also slightly promote the *J*_{sc} and FF of BTTIC-2M-based OSCs, which is due that the methyl group lift the LUMO level and also enhances the intermolecular packing and thus regulates the morphology of the active layer. Although PBDB-T:BTTIC-4M realized a higher *V*_{oc} (obtaining a very low *E*_{loss} of 0.52 eV when paired with PBDB-T), the overall performance is poor due to the low *J*_{sc} and FF. As predicted by theoretical calculations, too much methyl (BTTIC-4M) on the end group will damage the planarity of the SMA and induce interaction with the polymer causing poor morphology of BHJ layer, and the improved exciton bonding energy will also reduce the exciton dissociation efficiency, which will significantly lower the *J*_{sc} and FF (this part will be discussed in detail below). BTTIC-2M is actually a compromise between BTTIC-0M and BTTIC-4M in balancing current-voltage losses and adjusting microtopography, realizing three relatively balanced parameters in the applications of OSCs. In addition, the average values with mean square errors calculated from 20 devices of PCEs are 11.50% ± 0.22%, 12.68% ± 0.31% and 9.28% ± 0.17% for the PBDB-T:BTTIC-0M-, PBDB-T:BTTIC-2M- and PBDB-T:BTTIC-4M-based OSCs, indicative of great repeatability of the device fabrication. The long-term stability of best-performing OSCs based on PBDB-T:BTTIC-2M was tested with the conventional devices packaged and placed in air, and the stability curve is shown in Fig. S2. It can be seen that the PCEs of OSCs based on PBDB-T:BTTIC-2M dropped fast in the first three days, and then the rate of decline slowed down. The OSCs can maintain 85.8% PCE after 5 days, 83.6% PCE after 10 days, 80.5% PCE after 15 days and even 72.2% PCE after 30 days relative to the original PCE (13.15%), indicating good device stability.

2.5. Devices characterization

The charge transport behaviors of three SMAs in their neat and blend films were investigated by fabricating the hole-only (with a structure of ITO/V₂O₅/active layer/V₂O₅/Al) and electron-only diodes (with a structure of ITO/ZnO/active layer/ZrAcac/Al). By fitting the data using space charge limited current (SCLC) model (Fig. S3), the electron mobilities of BTTIC-0M, BTTIC-2M and BTTIC-4M were estimated to be 6.73 × 10⁻⁴, 8.19 × 10⁻⁴ and 9.38 × 10⁻⁴ cm² V⁻¹ s⁻¹, respectively, suggesting methyl groups help favorable π-π stackings which agrees well with the calculated BEs for their dimer molecules. When coming into the blend films (PBDB-T with a hole mobility of 1.08 × 10⁻³ cm² V⁻¹ s⁻¹), the hole (*μ*_h)/electron (*μ*_e) mobilities are 6.21 × 10⁻⁴/3.67 × 10⁻⁴ cm² V⁻¹ s⁻¹, 6.91 × 10⁻⁴/4.61 × 10⁻⁴ cm² V⁻¹ s⁻¹ and 8.05 × 10⁻⁴/3.96 × 10⁻⁴ cm² V⁻¹ s⁻¹ with *μ*_h/*μ*_e of 1.69, 1.50 and 2.03 for the PBDB-T:BTTIC-0M,

Table 2 The photovoltaic parameters of three SMAs-based OSCs.View Article Online
DOI: 10.1039/C9TA00597H

Active layer	V_{oc} (V) ^{a)}	J_{sc} (mA cm ⁻²) ^{a)}	FF (%) ^{a)}	PCE (%) ^{a)}
PBDB-T:BTTIC-0M	0.860 (0.850 ± 0.006)	18.95 (18.71 ± 0.21)	72.9 (72.3 ± 1.1)	11.87 (11.50 ± 0.22)
PBDB-T:BTTIC-2M	0.900 (0.896 ± 0.005)	19.39 (19.38 ± 0.20)	75.3 (73.1 ± 1.6)	13.15 (12.68 ± 0.31)
PBDB-T:BTTIC-4M	0.968 (0.968 ± 0.003)	15.67 (15.51 ± 0.21)	63.7 (61.8 ± 1.6)	9.60 (9.28 ± 0.17)

^{a)}The values in parenthesis are average values and mean square errors calculated from 20 devices.

PBDB-T:BTTIC-2M and PBDB-T:BTTIC-4M, respectively. The relatively balanced carriers mobility of PBDB-T:BTTIC-2M is beneficial to reduce the bimolecular recombination and achieve better J_{sc} and FF in OSCs.

For a further understanding, the exciton dissociation and charge extraction properties of optimal OSCs were studied by plotting the photocurrent density (J_{ph}) versus effective applied voltage (V_{eff}). As shown in Fig. 3d, the J_{ph} can quickly reach saturation (J_{sat}) at about 0.5 V. The J_{sat} s for PBDB-T:BTTIC-0M-, PBDB-T:BTTIC-2M- and PBDB-T:BTTIC-4M-based OSCs are found to be 19.82 mA cm⁻², 20.43 mA cm⁻² and 17.28 mA cm⁻², respectively, indicating a largest maximum exciton generation rate (G_{max}) of PBDB-T:BTTIC-2M according to $J_{sat} = qLG_{max}$ where q is the elementary charge and L is the thickness of active layer. Generally, the probabilities of exciton dissociation (P_{diss}) and charge extraction collection (P_{coll}) of OSCs can be evaluated by the ratios of J_{ph}/J_{sat} at short circuit and maximal power output conditions, respectively. The P_{diss} s and P_{coll} s are 95.6/85.0% for PBDB-T:BTTIC-0M, 94.9/85.2% for PBDB-T:BTTIC-2M and 90.1/78.5% for PBDB-T:BTTIC-4M, respectively. The P_{diss} of PBDB-T:BTTIC-2M is similar to that of PBDB-T:BTTIC-0M and obviously greater than that of PBDB-T:BTTIC-4M, which is consistent with the calculated exciton BEs. In addition, we also measured the photocurrent (J_{ph}) as a function of light intensities (P) to understand the bimolecular recombination in the optimal OSCs based on three SMAs. It can be clearly seen that the J_{ph} is highly linear dependence on P with the slopes (S) being 0.96, 0.97 and 0.90 for BTTIC-0M-, BTTIC-2M- and BTTIC-4M-based OSCs (Fig. 3e). The more serious charge recombination in PBDB-T:BTTIC-4M-based OSCs may result from multiscale phase separation in the blend films, which account for the low FF and J_{sc} of BTTIC-4M-based OSCs.

The external quantum efficiency (EQE) as a function of wavelength is defined as the ratio of collected photogenerated carriers and the number of incident photon, and it is determined by the product of efficiencies of absorption (A), exciton diffusion (ED), charge separation (CS), charge transport (CT) and charge collection (CC), giving $EQE = \eta_A \times \eta_{ED} \times \eta_{CS} \times \eta_{CT} \times \eta_{CC}$. As shown in Fig. 2c, the PBDB-T:BTTIC-2M-based OSCs shows a slightly higher EQE than that of PBDB-T:BTTIC-0M-based OSCs and a much higher EQE than that of PBDB-T:BTTIC-4M-based OSCs. Although the similar η_{CS} and η_{CC} between BTTIC-0M and BTTIC-2M-based OSCs, the BTTIC-2M-based OSCs still exhibits a higher EQE, indicating a higher η_{ED} and η_{CT} in BTTIC-2M-based OSCs than that in BTTIC-0M-based OSCs (assuming the same η_A). Moreover, excessive methyl groups (BTTIC-4M) not only affect η_{CS} and η_{CC} of OSCs, but also reduce η_{ED} and η_{CT} owing to poor morphology. The EQE-integrated J_{sc} s

are 18.67 mA cm⁻², 19.10 mA cm⁻² and 15.20 mA cm⁻² for the PBDB-T:BTTIC-0M-, PBDB-T:BTTIC-2M- and PBDB-T:BTTIC-4M-based OSCs, which are consistent with the measured J_{sc} s within an error of 2%.

2.6. Morphology studies

Atomic force microscope (AFM) measurements were carried out to studied the surface morphology of BTTIC-0M, BTTIC-2M and BTTIC-4M neat and blend films, and corresponding AFM height sensor images are shown in Fig. 4a-f. The neat films of BTTIC-0M, BTTIC-2M and BTTIC-4M all exhibit smooth and uniform morphology with small root-mean-square (RMS) roughness of 0.45, 0.41 and 0.38 nm, respectively, indicating a good film-forming ability of three SMAs. When PBDB-T was incorporated, the RMS roughnesses were increased into 1.27, 1.37 and 4.11 nm, respectively. It can be clearly observed that a good phase separation and an interpenetrating nanofiber microstructure are formed and developed in PBDB-T:BTTIC-0M and PBDB-T:BTTIC-2M blend films, which is beneficial to the effective processes of exciton dissociation and charge

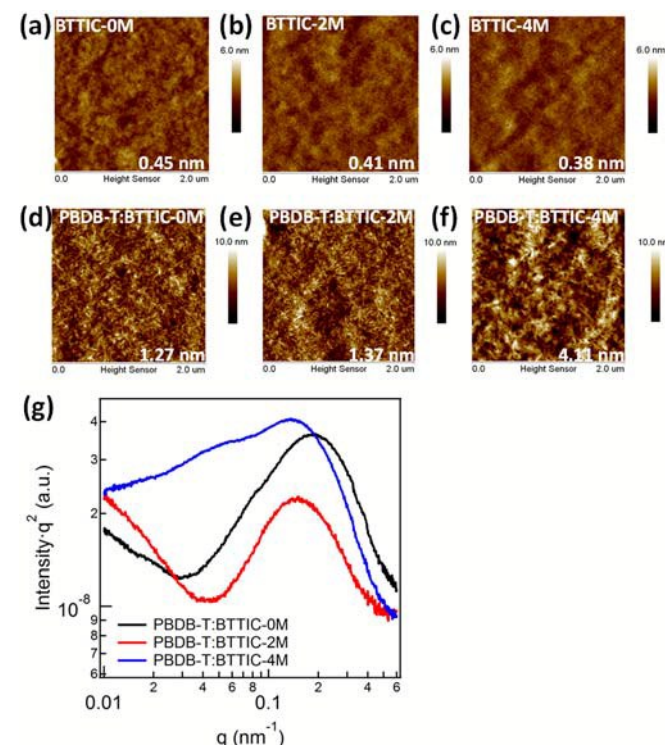


Fig. 4 The AFM height sensor images (2 $\mu\text{m} \times 2 \mu\text{m}$): a) BTTIC-0M neat film; b) BTTIC-2M neat film; c) a BTTIC-4M neat film; d) a PBDB-T:BTTIC-0M blend film; e) a PBDB-T:BTTIC-2M blend film; f) a PBDB-T:BTTIC-4M blend film. g) RSoXS profiles of optimal blend films based on three SMAs.

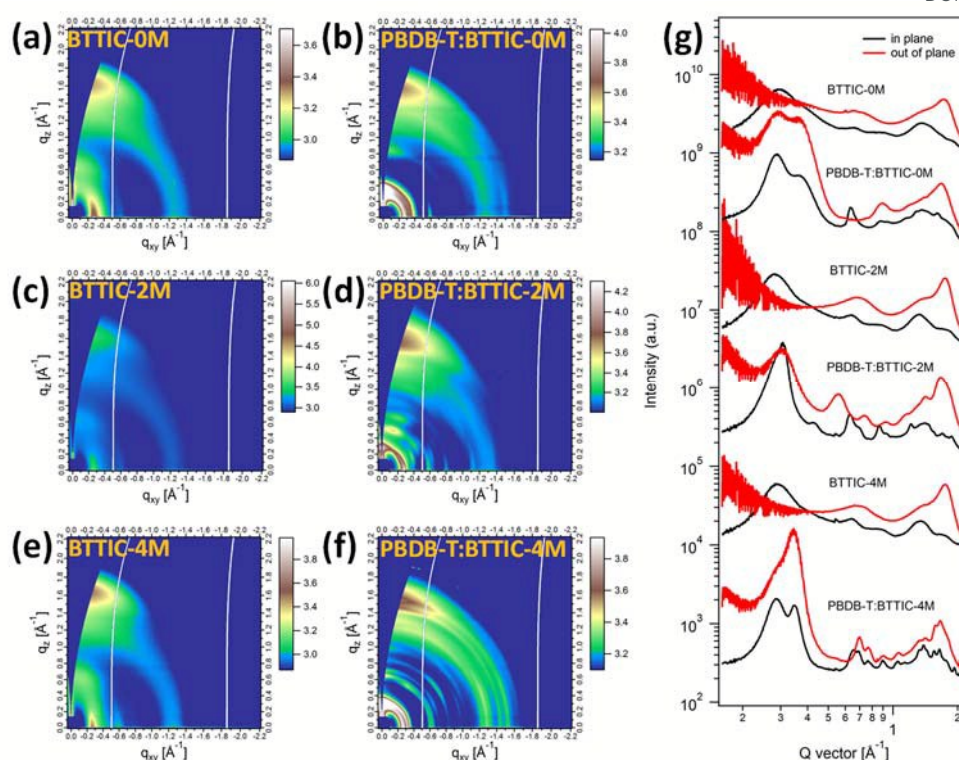


Fig. 5 The 2D-GIWAXS patterns: a) a BTTIC-0M neat film; b) a PBDB-T:BTTIC-0M blend film; c) a BTTIC-2M neat film; d) a PBDB-T:BTTIC-2M blend film; e) a BTTIC-4M neat film; f) a PBDB-T:BTTIC-4M blend film. g) Corresponding in-plane and out-of-plane cut-line profiles.

transport and thus enhance the J_{SC} and FF of OSCs. A great RMS change from BTTIC-4M neat film to blend film reveals that PBDB-T components may disrupt the ordered packing of BTTIC-4M and lead to a rough morphology. Resonant soft X-ray scattering (RSoXS) experiments were also performed to observe the domain size and purity of three optimal active layers (Fig. 4g). A similar and high domain purity and a moderate domain size (18 nm) appear in PBDB-T:BTTIC-0M and PBDB-T:BTTIC-2M blend films, which is beneficial to reduce the bimolecular recombination for achieving large J_{SC} s and high FFs in OSCs. Interestingly, two different domain sizes, namely a small-scale phase and (20 nm) a large-scale phase (56 nm), can be observed in PBDB-T:BTTIC-4M blend film. The large-scale phase is very likely caused by the interaction between PBDB-T and BTTIC-4M, and the small-scale phase is the normal size slightly bigger than those of PBDB-T:BTTIC-0M and PBDB-T:BTTIC-2M. However, the non-uniform phase will significantly reduce the phase purity and large-scale phase will hinder the exciton dissociation and increase the probability of recombination, which are responsible for the low J_{SC} and FF of BTTIC-4M based OSCs.

To gain insights into the inner intermolecular packing of three SMAs in their neat and blend films, the grazing-incidence wide angle X-ray scattering (GIWAXS) was studied, and the 2D-GIWAXS patterns and corresponding in-plane and out-of-plane cut-line profiles are shown in Fig. 5. In neat films, BTTIC-0M, BTTIC-2M and BTTIC-4M all exhibited intense (010) diffraction peaks in out-of-plane direction at about 1.74 \AA^{-1} (d -spacing of 3.61 \AA) and a (100) diffraction peaks in in-plane direction at

about 0.29 \AA^{-1} (d -spacing of 21.6 \AA), corresponding to a face-on orientation. The coherence lengths (CL) calculated from the lamellar packing and π - π stacking peaks are $62.80/21.81 \text{ \AA}$ for BTTIC-0M neat film, $69.78/23.79 \text{ \AA}$ for BTTIC-2M neat film and $69.01/25.53 \text{ \AA}$ for BTTIC-4M neat film, which informs us that adding methyl groups into the end groups can significantly enhance the packing properties of SMAs. When coming to the blend films, the face-on orientation does not change and the lamellar packing and π - π stacking were both enhanced. To better illustrate the role of methyl groups, we isolated the signals of donor and acceptor in blend films and analyzed them separately. The CLs of three SMAs in blend films calculated from in-plane and out-of-plane signal were $120.77/30.34 \text{ \AA}$ for BTTIC-0M, $165.26/41.59 \text{ \AA}$ for BTTIC-2M and $120.77/36.30 \text{ \AA}$ for BTTIC-4M, respectively. It should be noted that the better CLs of lamellar packing and π - π stacking of BTTIC-2M in blend film is beneficial for the horizontal and vertical transport of charges, resulting in a better electron mobility of PBDB-T:BTTIC-2M blend films compared to those of PBDB-T:BTTIC-0M and PBDB-T:BTTIC-4M blend films. According to the packing performance of three SMAs in pure films, the CL of BTTIC-4M in the blend film should be larger than that of BTTIC-2M, but it is significantly smaller than that of BTTIC-2M, revealing that the PBDB-T breaks up the order of molecule packing of BTTIC-4M. We also calculated the π - π stacking CLs of polymer donor in different blend films, being 27.42 \AA , 36.09 \AA and 63.43 \AA for PBDB-T in BTTIC-0M-, BTTIC-2M- and BTTIC-4M-nased blends, respectively. The largely increased CLs of PBDB-T in BTTIC-4M

blend film, multi-order diffraction halo (Fig. 5f) and significantly weakened π - π stacking of PBDB-T:BTTIC-4M blend film (Fig. 5g) provide solid evidences for interaction between PBDB-T and BTTIC-4M, forming a large-scale phase through a jaw-like structure of CPTCN-2M.

3. Conclusion

In conclusion, three SMAs, namely BTTIC-0M, BTTIC-2M and BTTIC-4M were designed and synthesized by adding methyl to the end group of CPTCN. A basis effect can be observed is that the LUMO level of BTTIC-0M, BTTIC-2M and BTTIC-4M were gradually elevated and the absorption spectra gradually shift blue with the increase of methyl groups, which will lead to a promoted V_{OC} and simultaneously a reduced J_{SC} in OSCs. In-depth theoretical calculations of dimer molecules and D-A complex revealed that methyl can significantly reduce the intermolecular recombination energy but increase the interface exciton binding energy at the same time. Compared with BTTIC-0M, BTTIC-2M show higher LUMO level without sacrificing the absorption. Moreover, although adding methyl group slightly increases the exciton BE of BTTIC-2M-based D-A complex and results in a slightly reduced exciton dissociation efficiency of PBDB-T:BTTIC-2M blend film, the enhanced π - π stacking optimizes the BHJ morphology and help to achieve a higher and more balanced carrier mobility and smaller bimolecular recombination in PBDB-T:BTTIC-2M-based active layer than those of PBDB-T:BTTIC-0M, which leads to an enhancement of J_{SC} and FF, and thus highest PCE over 13% in OSC based on PBDB-T:BTTIC-2M. In BTTIC-4M, the ipsilateral methyl and cyano groups form a sterically hindered jaw that induces interactions between polymer and BTTIC-4M, which leads to a significant absorption blue-shift over 50 nm and poor morphology (rough surface, different scale phase separation and weakened π - π stacking) of PBDB-T:BTTIC-4M blend film, resulting in lowest J_{SC} , FF and PCE among three OSCs. In general, by adjusting the amount of methyl added to the SMAs, we compromised the current-voltage loss and optimized the BHJ morphology to achieve 13% efficiency in OSCs.

Conflicts of interest

There are no conflicts to declare.

Acknowledgements

W. Gao and T. Liu contributed equally to this work. This work was financially supported by the National Natural Science Foundation of China (No. 21572171, 21504066 and 21534003), the National Basic Research Program of China (973 Program project numbers 2013CB834701 and 2014CB643501), the Shenzhen Technology and Innovation Commission (project number JCYJ20170413173814007), Ministry of science and technology (No. 2016YFA0200700). X-ray data was acquired at beamlines 7.3.3 and 11.0.1.2 at the Advanced Light Source, The

authors thank Chenhui Zhu at beamline 7.3.3, and Cheng Wang at beamline 11.0.1.2 for assistance with data acquisition.

Notes and references

- G. Yu, J. Cao, J. C., Hummelen, F. Wudl and A. J. Heeger, *Science*, 1995, **270**, 1789-1791.
- A. J. Heeger, *Adv. Mater.*, 2014, **26**, 10-28.
- L. Lu, T. Zheng, Q. Wu, A. M. Schneider, D. Zhao and L. Yu, *Chem. Rev.*, 2015, **115**, 12666-12731.
- B. C. Thompson and J. M. J. Fréchet, *Angew. Chem. Int. Ed.*, 2008, **47**, 58-77.
- F. C. Krebs, *Sol Energy Mat Sol C*, 2009, **93**, 394-412.
- H. Yao, L. Ye, H. Zhang, S. Li, S. Zhang and J. Hou, *Chem. Rev.*, 2016, **116**, 7397-7457.
- J. Hou, M.-H. Park, S. Zhang, Y. Yao, L.-M. Chen, J.-H. Li and Y. Yang, *Macromolecules*, **2008**, **41**, 6012-6018.
- J. Subbiah, B. Purushothaman, M. Chen, T. Qin, M. Gao, D. Vak, F. H. Scholes, X. Chen, S. E. Watkins, G. J. Wilson, A. B. Holmes, W. W. Wong and D. J. Jones, *Adv. Mater.* 2015, **27**, 702-705.
- Y. Liang, Z. Xu, J. Xia, S.-T. Tsai, Y. Wu, G. Li, C. Ray and L. Yu, *Adv. Mater.* 2010, **22**, E135-E138.
- D. Qian, L. Ye, M. Zhang, Y. Liang, L. Li, Y. Huang, X. Guo, S. Zhang, Z. a. Tan and J. Hou, *Macromolecules*, 2012, **45**, 9611-9617.
- Y. Zou, A. Najari, P. Berrouard, S. Beaupré, B. R. Aïch, Y. Tao and M. Leclerc, *J. Am. Chem. Soc.*, 2010, **132**, 5330-5331.
- S. C. Price, A. C. Stuart, L. Yang, H. Zhou and W. You, *J. Am. Chem. Soc.*, 2011, **133**, 4625-4631.
- J. Wolf, F. Cruciani, A. E. Labban and P. M. Beaujuge, *Chem. Mater.*, 2015, **27**, 4184-4187.
- L. Huo, T. Liu, X. Sun, Y. Cai, A. J. Heeger and Y. Sun, *Adv. Mater.*, 2015, **27**, 2938-2944.
- J. Zhao, Y. Li, G. Yang, K. Jiang, H. Lin, H. Ade, W. Ma and H. Yan, *Nat. Energy*, 2015, **1**, 15027.
- W. Gao, T. Liu, M. Hao, K. Wu, C. Zhang, Y. Sun and C. Yang, *Chem. Sci.*, 2016, **7**, 6167-6175.
- D. Zhu, X. Bao, Q. Zhu, C. Gu, M. Qiu, S. Wen, J. wang, B. Shahid and R. Yang, *Energy Environ. Sci.*, 2017, **10**, 614-620.
- X. Guo, N. Zhou, S. J. Lou, J. Smith, D. B. Tice, J. W. Hennek, R. P. Ortiz, J. T. L. Navarrete, S. Li, J. Strzalka, L. X. Chen, R. P. H. Chang, A. Facchetti and T. J. Marks, *Nat. Photonics*, 2013, **7**, 825-833.
- D. Deng, Y. Zhang, J. Zhang, Z. Wang, L. Zhu, J. Fang, B. Xia, Z. Wang, K. Lu, W. Ma and Z. Wei, *Nat. Commun.*, 2016, **7**, 13740.
- T. Kumari, S. M. Lee, S.-H. Kang, S. Chen and C. Yang, *Energy Environ. Sci.*, 2017, **10**, 258-265.
- C. Yan, S. Barlow, Z. Wang, H. Yan, A. K.-Y. Jen, S. R. Marder and X. Zhan, *Nat. Rev. Mater.*, 2018, **3**, 18003.
- J. Hou, O. Inganäs, R. H. Friend and F. Gao, *Nat. Mater.*, 2018, **17**, 119-128.
- Y. Lin, J. Wang, Z. G. Zhang, H. Bai, Y. Li, D. Zhu and X. Zhan, *Adv. Mater.*, 2015, **27**, 1170.
- Y. Lin, Q. He, F. Huo, J. Mai, X. Lu, C.-J. Su, T. Li, J. Wang, J. Zhu, Y. Sun, C. Wang and X. Zhan, *J. Am. Chem. Soc.*, 2016, **138**, 2973-2976.
- W. Wang, C. Yan, T.-K. Lau, J. Wang, K. Liu, Y. Fan, X. Lu and X. Zhan, *Adv. Mater.*, 2017, **29**, 1701308.
- T. Li, S. Dai, Z. Ke, L. Yang, J. Wang, C. Yan, W. Ma and X. Zhan, *Adv. Mater.*, 2018, **30**, 1705969.
- S. Dai, T. Li, W. Wang, Y. Xiao, T.-K. Lau, Z. Li, K. Liu, X. Lu and X. Zhan, *Adv. Mater.*, 2018, **30**, 1706571.
- W. Li, L. Ye, S. Li, H. Yao, H. Ade and J. Hou, *Adv. Mater.*, 2018, **30**, 1707170.

- 29 X. Song, N. Gasparini, L. Ye, H. Yao, J. Hou, H. Ade and D. Baran, *ACS Energy Lett.*, 2018, **3**, 669.
- 30 Z. Yao, X. Liao, K. Gao, F. Lin, X. Xu, X. Shi, L. Zuo, F. Liu, Y. Chen and A. K.-Y. Jen, *J. Am. Chem. Soc.*, 2018, **140**, 2054.
- 31 Z. Fei, F. D. Eisner, X. Jiao, M. Azzouzi, J. A. Röhr, Y. Han, M. Shahid, A. S. R. Chesman, C. D. Easton, C. R. McNeill, T. D. Anthopoulos, J. Nelson and M. Heeney, *Adv. Mater.*, 2018, **30**, 1705209.
- 32 F.-X. Chen, J.-Q. Xu, Z.-X. Liu, M. Chen, R. Xia, Y. Yang, T.-K. Lau, Y. Zhang, X. Lu, H.-L. Yip, A. K.-Y. Jen, H. Chen and C.-Z. Li, *Adv. Mater.*, 2018, **30**, 1803769.
- 33 W. Gao, T. Liu, R. Ming, Z. Luo, K. Wu, L. Zhang, J. Xin, D. Xie, G. Zhang, W. Ma, H. Yan and C. Yang, *Adv. Funct. Mater.*, 2018, **28**, 1803128.
- 34 J. Zhang, W. Liu, S. Chen, S. Xu, C. Yang and X. Zhu, *J. Mater. Chem. A*, 2018, **6**, 22519.
- 35 B. Gao, H. Yao, J. Hou, R. Yu, L. Hong, Y. Xu and J. Hou, *J. Mater. Chem. A*, 2018, **6**, 23644.
- 36 J. Yuan, Y. Zhang, L. Zhou, G. Zhang, H.-L. Yip, T.-K. Lau, X. Lu, C. Zhu, H. Peng, P. A. Johnson, M. Leclerc, Y. Cao, J. Ulanski, Y. Li and Y. Zou, *Joule*, 2019, **3**, 1.
- 37 S. Li, L. Ye, W. Zhao, S. Zhang, H. Ade and J. Hou, *Adv. Energy Mater.*, 2017, **7**, 1700183.
- 38 S. Li, L. Ye, W. Zhao, S. Zhang, S. Mukherjee, H. Ade and J. Hou, *Adv. Mater.*, 2016, **28**, 9423.
- 39 Z. Luo, H. Bin, T. Liu, Z.-G. Zhang, Y. Yang, C. Zhong, B. Qiu, G. Li, W. Gao, D. Xie, K. Wu, Y. Sun, F. Liu, Y. Li and C. Yang, *Adv. Mater.*, 2018, **30**, 1706124.
- 40 D. Xie, T. Liu, W. Gao, C. Zhong, L. Huo, Z. Luo, K. Wu, W. Xiong, F. Liu, Y. Sun and C. Yang, *Sol. RRL*, 2017, **1**, 1700044.
- 41 W. Gao, Q. An, R. Ming, D. Xie, K. Wu, Z. Luo, Y. Zou, F. Zhang and C. Yang, *Adv. Funct. Mater.*, 2017, **27**, 1702194.
- 42 Y. Lin, Q. He, F. Zhao, L. Huo, J. Mai, X. Lu, C.-J. Su, T. Li, J. Wang, J. Zhu, Y. Sun, C. Wang and X. Zhan, *J. Am. Chem. Soc.*, 2016, **138**, 2973.
- 43 T. Liu, Z. Luo, Q. Fan, G. Zhang, L. Zhang, W. Gao, X. Guo, W. Ma, M. Zhang, C. Yang, Y. Li and H. Yan, *Energy Environ. Sci.*, 2018, **11**, 3275.
- 44 W. Gao, T. Liu, C. Zhong, G. Zhang, Y. Zhang, R. Ming, L. Zhang, J. Xin, K. Wu, Y. Guo, W. Ma, H. Yan, Y. Liu and C. Yang, *ACS Energy Lett.*, 2018, **3**, 1760.
- 45 M. Zhang, W. Gao, F. Zhang, Y. Mi, W. Wang, Q. An, J. Wang, X. Ma, J. Miao, Z. Hu, X. Liu, J. Zhang and C. Yang, *Energy Environ. Sci.*, 2018, **11**, 841.
- 46 W. Gao, M. Zhang, T. Liu, R. Ming, Q. An, K. Wu, D. Xie, Z. Luo, C. Zhong, F. Liu, F. Zhang, H. Yan and C. Yang, *Adv. Mater.*, 2018, **30**, 1800052.
- 47 W. Gao, Q. An, C. Zhong, Z. Luo, R. Ming, M. Zhang, Y. Zou, F. Liu, F. Zhang and C. Yang, *Chem. Sci.*, 2018, **9**, 8142.
- 48 X. Ma, W. Gao, J. Yu, Q. An, M. Zhang, Z. Hu, J. Wang, W. Tang, C. Yang and F. Zhang, *Energy Environ. Sci.*, 2018, **11**, 2134.
- 49 Q. An, J. Zhang, W. Gao, F. Qi, M. Zhang, X. Ma, C. Yang, L. Huo and F. Zhang, *Small*, 2018, **14**, 1802983.
- 50 R. Lv, D. Chen, X. Liao, L. Chen and Y. Chen, *Adv. Funct. Mater.*, 2019, **29**, 1805872.
- 51 Y. Li, N. Zheng, L. Yu, S. Wen, C. Gao, M. Sun and R. Yang, *Adv. Mater.*, 2019, **31**, 1807832.
- 52 T. J. Aldrich, M. Matta, W. Zhu, S. M. Swick, C. L. Stern, G. C. Schatz, A. Facchetti, F. S. Melkonyan and T. J. Marks, *J. Am. Chem. Soc.*, 2019, DOI: 10.1021/jacs.8b13653.
- 53 X. Li, F. Pan, C. Sun, M. Zhang, Z. Wang, J. Du, J. Wang, M. Xiao, L. Xue, Z.-G. Zhang, C. Zhang, F. Liu and Y. Li, *Nat. Commun.*, 2019, **10**, 519.
- 54 X. Xu, T. Yu, Z. Bi, W. Ma, Y. Li and Q. Peng, *Adv. Mater.*, 2018, **30**, 1703973.
- 55 L. Meng, Y. Zhang, X. Wan, C. Li, X. Zhang, Y. Wang, X. Ke, Z. Xiao, L. Ding, R. Xia, H.-L. Yip, Y. Cao and Y. Chen, *Science*, 2018, **361**, 1094.
- 56 Z. Zheng, Q. Hu, S. Zhang, D. Zhang, J. Wang, S. Xie, R. Wang, Y. Qin, W. Li, L. Hong, N. Liang, F. Liu, Y. Zhang, Z. Wei, Z. Tang, T. P. Russell, J. Hou and H. Zhou, *Adv. Mater.*, 2018, **30**, 1801801.
- 57 T. Liu, L. Huo, S. Chandrabose, K. Chen, G. Han, F. Qi, X. Meng, D. Xie, W. Ma, Y. Yi, J. M. Hodgkiss, F. Liu, J. Wang, C. Yang and Y. Sun, *Adv. Mater.*, 2018, **30**, 1707353.
- 58 S. Li, L. Ye, W. Zhao, H. Yan, B. Yang, D. Liu, W. Li, H. Ade and J. Hou, *J. Am. Chem. Soc.*, 2018, **140**, 7159.
- 59 G. Liu, J. Jia, K. Zhang, X. Jia, Q. Yin, W. Zhong, L. Li, F. Huang and Y. Cao, *Adv. Energy Mater.*, 2019, **9**, 1803657.
- 60 K. Gao, S. B. Jo, X. Shi, L. Nian, M. Zhang, Y. Kan, F. Lin, B. Kan, B. Xu, Q. Rong, L. Shui, F. Liu, X. Peng, G. Zhou, Y. Cao and A. K.-Y. Jen, *Adv. Mater.*, 2019, **31**, 1807842.
- 61 L. Tan, Y. Wang, J. Zhang, S. Xiao, H. Zhou, Y. Li, Y. Chen and Y. Li, *Adv. Sci.*, 2019, **6**, 1801180.
- 62 X. Li, Y. Wang, Q. Zhu, X. Guo, W. Ma, X. Ou, M. Zhang and Y. Li, *J. Mater. Chem. A*, 2019, DOI: 10.1039/c8ta11441b.